

Progressive Quantum Algorithm for Maximum Independent Set with Quantum Alternating Operator Ansatz

Xiao-Hui Ni,^{1,2} Ling-Xiao Li,¹ Yan-Qi Song,³ Zheng-Ping Jin,^{1,2,4} Su-Juan Qin,^{1,2,4,*} and Fei Gao^{1,2,4,†}

¹*State Key Laboratory of Networking and Switching Technology,
Beijing University of Posts and Telecommunications, Beijing, 100876, China*

²*School of Cyberspace Security, Beijing University of Posts and Telecommunications, Beijing, 100876, China*

³*Security Research Department, China Academy of Information and Communications Technology, Beijing, China*

⁴*National Engineering Research Center of Disaster Backup and Recovery,
Beijing University of Posts and Telecommunications*

(Dated: September 27, 2024)

Recently, Hadfield et al. proposed the Quantum Alternating Operator Ansatz (QAOA+) to tackle Constrained Combinatorial Optimization Problems (CCOPs). This paper proposes a Progressive Quantum Algorithm (PQA) to reduce the required qubits in solving the Maximum Independent Set (MIS) problem using QAOA+ ansatz. PQA constructs a subgraph that contains the MIS solution of the target graph G and then solves the MIS problem on this subgraph to obtain the solution for G . To induce such a subgraph, PQA starts with a small-scale initial subgraph and progressively expands its graph size utilizing designed expansion rules. After each expansion, PQA solves the MIS problem on the current subgraph using QAOA+. In each run, PQA repeats the graph expansion and solving process until a predefined stopping condition is reached. Simulation results demonstrate that to achieve an optimal approximation ratio of 0.95, PQA requires only 5.5565% (15.4%) of the qubits and 10.695% (7.23%) of the runtime compared with QAOA+ on Erdős-Rényi (regular) graphs, highlighting the efficiency of PQA.

I. INTRODUCTION

Over recent years, quantum computing has emerged as a promising computational paradigm, demonstrating its potential for addressing complex problems such as database searching [1], prime factorization [2], data dimension reduction [3–6] and solving equations [7]. However, the practical implementation of these quantum algorithms is hindered by noise and the limited qubit capacity of existing Noisy Intermediate-Scale Quantum (NISQ) devices [8–10]. Therefore, hybrid quantum-classical algorithms [11–20] have been proposed to harness the capabilities of NISQ devices more effectively.

The Quantum Approximate Optimization Algorithm (QAOA) [21–29] is a hybrid quantum-classical algorithm with broad applications. Specifically, it has been used to solve the exact cover [30], vertex cover [31], and other Combinatorial Optimization Problems (COPs) [32–36]. Constrained COPs (CCOPs) are a crucial subclass of combinatorial optimization, and solving CCOPs requires not only finding the optimal solution but also satisfying specific constraints, making them more complex and challenging compared with Unconstrained COPs (UCOPs) [37]. To address these challenges for solving CCOPs, Hadfield et al. [38] proposed an improved version of the original QAOA [21], known as QAOA+.

QAOA+ constructs a Hilbert space that only contains feasible solutions to the problem, thereby reducing the solution search space compared with the original QAOA [33]. Currently, QAOA+ has been applied to solve Maximum Independent Set (MIS) [39], minimum exact cover [40] and other CCOPs [41–43].

Given the limited resources of NISQ devices, developing heuristic strategies to reduce the qubit requirements of QAOA+ in solving CCOPs becomes essential. Recently, Tomesh et al. [44] proposed Quantum Local Search (QLS) with the QAOA+ ansatz and studied its performance on the MIS problem. Different from directly solving the MIS problem using QAOA+ (DS-QAOA+) [39], QLS constructs a global solution by iterating through many local subproblems. Specifically, QLS constructs multiple local subgraphs (that may be of indeterminate graph size) based on certain strategies and solves the MIS problem on these subgraphs using QAOA+ to obtain local solutions. These local solutions are combined to form a global solution using classical methods. For DS-QAOA+, several qubits equal to the size of the graph are required. By breaking the problem into smaller subgraphs, QLS reduces the number of qubits needed for the MIS problem.

Inspired by the Proactively Incremental Learning (PIL) algorithm [45], a new method called the Progressive Quantum Algorithm (PQA) is proposed to reduce the required qubits for solving the MIS problem. PQA aims to construct a subgraph containing the MIS solution of the original problem and then solve the MIS problem

* qsjujuan@bupt.edu.cn

† gaof@bupt.edu.cn

on this subgraph to obtain the final solution. Specifically, PQA starts with a small, sparse initial subgraph and progressively expands its size following rules distinct from QLS. After each expansion, PQA solves the MIS problem on the newly generated subgraph using QAOA+. In each run, PQA repeats the graph expansion and solving process until a predefined stopping condition is reached. By doing so, PQA may solve the original MIS problem on a smaller-scale subgraph compared with DS-QAOA+, and it does not require reconstructing the global solution from multiple local solutions compared with QLS.

In our simulations, we compare the total qubits and runtime consumed by PQA, QLS, and DS-QAOA+ on multiple Erdős-Rényi (ER) and $k (= 2, 3)$ -regular graphs when they achieve the same optimal approximation ratio (OAR). **Across all tested graphs, PQA usually achieves the same OAR with fewer qubits and runtime than DS-QAOA+ and QLS.** Specifically, for an OAR of 0.95, PQA uses 5.5565% (26.77%) of the qubits required by DS-QAOA+ (QLS) on ER graphs, and 15.4% (52.605%) on regular graphs, respectively. Additionally, PQA reaches the same OAR in 10.695% (75.365%) of the runtime required by DS-QAOA+ (QLS) on ER graphs, and 7.23% (63.91%) on regular graphs. The MIS problem is one of the most widely studied CCOPs, partly due to its broad applicability in various domains and its equivalence to the minimum vertex cover and maximum clique. The efficiency of PQA in solving the MIS problem not only may enhance the practicality of quantum algorithms but also pave the way for solving larger-scale problems in the future.

This paper is structured as follows: Section II serves as the foundational segment, providing background knowledge on the MIS problem, QAOA, and its extension, QAOA+. Following this, in Section III, we delineate the progressive quantum algorithm, emphasizing the construction rules of the desired derived subgraph. Subsequently, in Section IV, we present a comprehensive set of numerical simulation experiments aimed at showcasing the quantum resource efficiency of PQA over DS-QAOA+ and QLS. Finally, in Section V, we offer a succinct conclusion and discussion to encapsulate the key findings of our study and the next research direction.

II. PRELIMINARIES

In this section, we introduce some preliminaries to help readers understand our work better.

A. Review of MIS

MIS is defined on a graph $G = (V, E)$, where $V = \{0, \dots, n - 1\}$ represents the set of vertices, and $E = \{(u, v)\}$ represents the set of edges, with the two vertices u and v on the edge (u, v) being adjacent. In this

paper, we denote the number of vertices and edges as n and m , respectively. A vertex subset V_s is called an independent set of G if no two vertices in V_s are adjacent. The MIS is the vertex subset with the largest number of vertices among all independent sets, and the number of vertices in the MIS is known as the independence number, denoted as $\beta(G)$ [37]. While the solution to MIS for a graph G may not be unique, the independence number is always determined.

For any target graph G , the independent vertex subsets in an induced subgraph G_q of G are feasible solutions for G . There is at least one induced subgraph $G_q = (V_q, E_q)$ that has an identical MIS solution to G , where $V_q \subseteq V$ and $E_q \subseteq E$. As illustrated in FIG. 1, the right graph is the induced subgraph of the left graph, and they have the same MIS solution $\{1, 2, 3\}$, but the MIS solution $\{1, 2, 4\}$ to FIG 1(a) is not the MIS solution of FIG. 1(b) because the node 4 is not in this induced subgraph. This implies that the MIS solution of the target graph may not always be a solution for its induced subgraph, and an independent set in G may not be feasible for G_q .

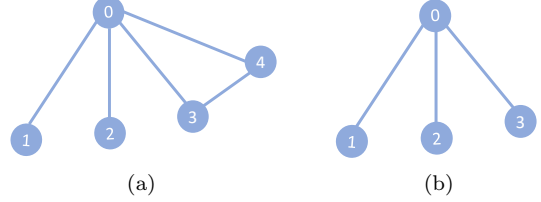


FIG. 1. Examples of MIS. (a) A target graph G whose feasible solutions are $\emptyset, \{0\}, \{1\}, \{2\}, \{3\}, \{4\}, \{1, 2\}, \{1, 3\}, \{1, 4\}, \{2, 3\}, \{2, 4\}, \{1, 2, 3\}$ and $\{1, 2, 4\}$. The solutions of MIS are $\{1, 2, 3\}$ and $\{1, 2, 4\}$, where the MIS solutions of G are not unique, but the independence number identically equals 3. (b) An induced subgraph of G and its MIS solution is $\{1, 2, 3\}$. The feasible solutions of G_q are $\emptyset, \{0\}, \{1\}, \{2\}, \{3\}, \{1, 2\}, \{1, 3\}, \{2, 3\}, \{1, 2, 3\}$. We respectively denote the feasible space including all feasible solutions of G_q and G as $S(G_q)$ and $S(G)$, where $S(G_q) \subseteq S(G)$.

In this paper, we utilize $x_u = 1$ to represent that the vertex u is in the vertex subset, otherwise, $x_u = 0$, where $u = 0, 1, \dots, n - 1$. Each way of vertex partition corresponds to a unique bit string x , and there are 2^n forms for x in total, where $x = x_0x_1 \dots x_{n-1}$. The goal for MIS is to maximize the objective function

$$C_1(x) = \sum_{u=0}^{n-1} x_u \quad (1)$$

when the independence constraint $\sum_{(u,v) \in E} x_u x_v = 0$ is met. This constraint can be incorporated into the objective function using the Lagrange multiplier method [46], thus converting the constrained problem to unconstrained problem. The obtained classical cost function

is

$$\max C(x) = \sum_{u=0}^{n-1} x_u - \lambda \sum_{(u,v) \in E} x_u x_v, \quad (2)$$

where the value of λ is determined through additional hyper-parameter optimization steps [36], and $\lambda > 1$ can impose penalties on those terms that violate independence constraints [47], making the maximal cost function value correspond to the exact MIS solution instead of other feasible or infeasible bit strings. Here, C_{\max} equals the independence number $\beta(G)$.

B. Review of QAOA

Inspired by quantum adiabatic evolution [48], QAOA encodes the solution of the problem into the ground state of the target Hamiltonian H_C and aims to gradually evolve towards this ground state through a parameterized quantum circuit (PQC). This evolution starts from the ground state $|s\rangle$ of the initial Hamiltonian H_B , with a quantum circuit built using p -level QAOA ansatz. Notably, the initial state $|s\rangle$ is required to be trivial to implement. That is, $|s\rangle$ can be prepared by a constant-depth quantum circuit.

For the original QAOA, one level QAOA ansatz consists of two variational QAOA parameters (denoted as γ_i and β_i) and two unitaries $e^{-i\gamma_i H_C}$ and $e^{-i\beta_i H_B}$, where $i = 1, 2, \dots, p$, and p is the level depth. Generally, the initial Hamiltonian is chosen as $H_B = -\sum_{u=0}^{n-1} \sigma_u^x$ because its ground state $|s\rangle = |+\rangle^{\otimes n}$ can be trivial to prepare. Here, σ_u^x refers to the Pauli-X operator applied to the u -th qubit, effectively flipping its state. To encode the MIS solution into the ground state of H_C , the cost function $-C(x)$ is transformed into the target Hamiltonian

$$H_C = \sum_{u=0}^{n-1} \frac{\sigma_u^z - I}{2} + \lambda \sum_{(u,v) \in E} \frac{I - \sigma_u^z - \sigma_v^z + \sigma_u^z \sigma_v^z}{4} \quad (3)$$

by transforming each binary variable x_u to a quantum spin $\frac{I - \sigma_u^z}{2}$ [21], where σ_u^z refers that applying Pauli-Z to the u -th qubit.

The ground state of H_C can be approximately obtained by alternately applying unitaries operators $e^{-i\gamma_i H_C}$ and $e^{-i\beta_i H_B}$ to the initial quantum state $|s\rangle$. After applying these unitaries for p levels (corresponding to $i = 1, 2, \dots, p$), the output state of the PQC is

$$|\gamma_p, \beta_p\rangle = \prod_{i=1}^p e^{-i\beta_i H_B} e^{-i\gamma_i H_C}, \quad (4)$$

where $\gamma_p = (\gamma_1, \dots, \gamma_p)$ and $\beta_p = (\beta_1, \dots, \beta_p)$ are $2p$ variational QAOA parameters. The expectation value $F(\gamma_p, \beta_p)$ of H_C in this variational quantum state is de-

fined as

$$F(\gamma_p, \beta_p) = -\langle \gamma_p, \beta_p | H_C | \gamma_p, \beta_p \rangle, \quad (5)$$

which can be calculated by repeated measurements of the output quantum state using the computational basis, and the goal is to search for the global optimal parameters

$$(\gamma_p^{opt}, \beta_p^{opt}) = \arg \max_{(\gamma_p, \beta_p)} F(\gamma_p, \beta_p). \quad (6)$$

The search for optimal parameters is typically done by starting with some guesses of the initial parameters, where the quantum computer computes the expectation value of the output state and delivers the relevant information to the classical computer. These parameters are optimized by the classical optimizer and then delivered to the quantum computer. The outer parameter optimization is repeated until it meets the termination condition (e.g., the maximal number of iterations or convergence tolerance ε [27]). To quantify the quality of the QAOA solution (i.e., measure the difference between the output state of QAOA and the ground state of H_C), we introduce the approximation ratio (AR)

$$r = \frac{F(\gamma_p, \beta_p)}{F_{\max}}, \quad (7)$$

where F_{\max} is the negative of the ground state energy of H_C , with equaling C_{\max} . For small graph instances, F_{\max} can be obtained by brute force search. For large graphs, an approximation of F_{\max} can be obtained by executing multiple runs of the greedy algorithm [49] and selecting the largest independent set found across these runs. AR reflects how close the solution provided by QAOA is to the exact solution, $r \leq 1$, with the value of 1 as the exact solution.

C. Review of QAOA+

The original QAOA searches for the ground state of H_C from a Hilbert space that includes both feasible and infeasible quantum states. As a result, the output states may not always satisfy the independence constraint and violate one or more constraints [33, 36]. To overcome this challenge, Hadfield et al. [38, 41] introduce a novel quantum alternating operator denoted as QAOA+.

Different from incorporating the independence constraint into the target Hamiltonian utilizing the Lagrange multiplier, QAOA+ encodes constraints into the mixer Hamiltonian H_B . This allows QAOA+ to search for the optimal solution within a feasible subspace that only contains feasible quantum states. Consequently, the target Hamiltonian

$$H_C = \sum_{u=0}^{n-1} \frac{\sigma_u^z - I}{2} \quad (8)$$

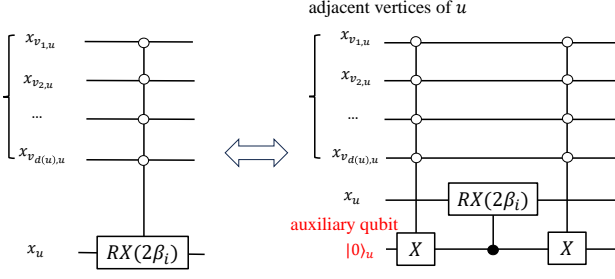


FIG. 2. The implementation of $e^{-i\beta_i B_u}$ when $d(u) \geq 1$. The multi-qubit controlled RX gate can be decomposed into two multi-qubit controlled gates and a single-qubit controlled RX gate, utilizing an auxiliary qubit [50]. The auxiliary qubit is initialized as $|0\rangle$ and is flipped to $|1\rangle$ only when the quantum states of all adjacent vertices are $|0\rangle$ (i.e., $f(u) = 0$). Once this condition is met, an RX gate is applied on the u -th qubit. After the operation, the state of the auxiliary qubit can be reset from $|1\rangle$ to $|0\rangle$ using the right multi-qubit controlled gate operation. Otherwise, the auxiliary qubit is always $|0\rangle$ when $f(u) > 0$, and there is an Identity operation applied to the u -th qubit.

is obtained by converting the x_u in $-C_1(x)$ to a quantum spin $\frac{I - \sigma_z}{2}$, thereby encoding the MIS solution into the ground state of H_C . Similar to QAOA, QAOA+ approaches the ground state of H_C by alternately applying unitaries $e^{-i\gamma_i H_C}$ and $e^{-i\beta_i H_B}$ on an initial quantum state $|s\rangle$ required to be trivial to implement. However, in QAOA+, the initial quantum state must be the superposition of feasible states. This requirement ensures that the feasible subspace contains no states that violate the constraints. In addition, the initial quantum state $|s\rangle$ may not be the ground state of H_B in QAOA+, unlike in QAOA.

The design of the mixing Hamiltonian H_B must preserve the feasibility of the subspace (i.e., ensure the subspace only has quantum states obeying constraints) and explore a new feasible subspace (i.e., provide transitions between various feasible states) [38]. For an independent vertex subset V_s , deleting an arbitrary vertex v_a (i.e., the state of x_{v_a} is converted from 1 to 0) from V_s does not change its independence. However, a new vertex v_a can be added to V_s (i.e., flipping x_{v_a} from 0 to 1) without destroying its independence only when there are no adjacent vertices of v_a in V_s . Thus, for any node, controlling its bit-flip operation based on the states of its neighbors is sufficient to both add and remove vertices while preserving the independence property [38]. The bit-flip of v_a occurs only if

$$f(v_a) = \sum_{j=1}^{d(v_a)} x_{v_{j,a}} = 0, \quad (9)$$

where $v_{j,a}$ is the j -th adjacent vertex of v_a , and $d(v_a)$ is the number of adjacent vertices of v_a , with $j =$

$1, \dots, d(v_a)$. Mapping to a quantum circuit, for any vertex u , a Pauli-X operation is applied on the u -th qubit (i.e., this qubit is flipped) if and only if all quantum states of adjacent vertices of u are $|0\rangle$ (i.e., $f(u) = 0$). Otherwise, a Pauli-I operation is applied on the u -th qubit. The corresponding partial mixer Hamiltonian B_u can be described as

$$B_u = \sum_{f(u)=0} |x_{v_{1,u}} \dots x_{v_{d(u),u}}\rangle \langle x_{v_{1,u}} \dots x_{v_{d(u),u}}| \otimes \sigma_u^x + \sum_{f(u)>0} |x_{v_{1,u}} \dots x_{v_{d(u),u}}\rangle \langle x_{v_{1,u}} \dots x_{v_{d(u),u}}| \otimes I. \quad (10)$$

The mixer Hamiltonian is given by $H_B = \sum_{u=0}^{n-1} B_u$. Specifically, the quantum state resulting from applying $e^{-i\beta_i B_u}$ to the single feasible quantum state $|x_o\rangle$ is

$$e^{-i\beta_i B_u} |x_o\rangle = \begin{cases} RX(2\beta_i) |x_o\rangle, & f(u) = 0 \\ |x_o\rangle, & f(u) > 0, \end{cases} \quad (11)$$

where the detailed result of $RX(2\beta_i) |x_o\rangle$ is $\cos 2\beta_i |x_o\rangle - i \sin 2\beta_i |x_0 \dots \bar{x}_u \dots x_{n-1}\rangle$, and \bar{x}_u denotes the state of u -th qubit is converted from $|0\rangle$ to $|1\rangle$ (or $|1\rangle$ to $|0\rangle$), implementing the addition or removal of node u without generating infeasible quantum states. The quantum circuit for $e^{-i\beta_i B_u}$, shown in FIG. 2, corresponds to a multi-qubit controlled RX gate when the node has $d(u) \geq 1$ adjacent vertices, and to a single RX gate when $d(u) = 0$. To help readers understand our subsequent work better, FIG. 3 provides a schematic illustrating the process of directly solving the MIS problem on the target graph using QAOA or QAOA+. Additionally, Table I is provided to clearly illustrate the differences between using QAOA and QAOA+ to solve the MIS problem.

III. PROGRESSIVE QUANTUM ALGORITHM

Any arbitrary graph has at least one induced subgraph with the same MIS solution as it. Based on this property, PQA iteratively constructs a derived subgraph that includes the MIS solution of G but is smaller in graph size. Naturally, solving the MIS problem on this subgraph requires fewer resources than directly solving it on the original graph. However, multiple derived subgraphs may exist, each with a different size but sharing the same MIS solution as G . As a result, various numbers of quantum gates and qubits are needed to implement the p -level QAOA+ ansatz for each subgraph.

Fewer quantum gates and qubits are required in the realization of $e^{-i\beta_i H_B}$ and $e^{-i\gamma_i H_C}$ as the number of nodes and edges decreases. Especially, in the realization of $e^{-i\beta_i H_B}$, multiple $d(v)$ -qubit controlled RX gates may be required. The overhead of implementing the $d(v)$ -qubit controlled RX gate is costly but decreases when the node v has fewer neighborhood nodes (i.e., a smaller

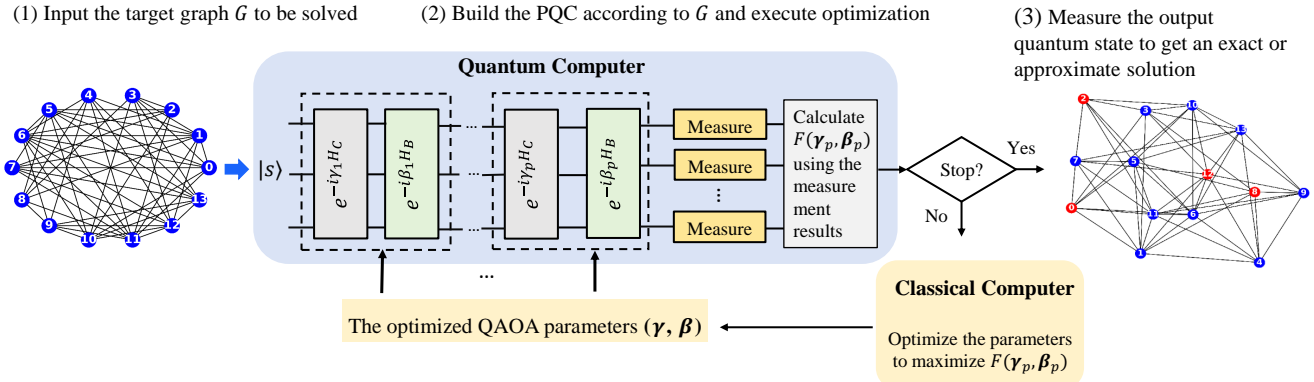


FIG. 3. A schematic of directly solving the MIS problem on the target graph using QAOA or QAOA+ ansatz, where the concrete form of the initial quantum state $|s\rangle$, the mixer Hamiltonian H_B , and the target Hamiltonian H_C are relevant to the choose of ansatz.

TABLE I. The difference between QAOA and QAOA+ when solving the MIS problem

	QAOA	QAOA+
Manipulation of constraint	Add it into H_C by Lagrange multiplier	Encode it into H_B
Initial state $ s\rangle$	$ s\rangle = +\rangle^{\otimes n}$	The superposition of feasible solutions
Mixer Hamiltonian H_B	$H_B = -\sum_{u=0}^{n-1} \sigma_u^x$	$H_B = \sum_{u=0}^{n-1} B_u$
Target Hamiltonian H_C	$H_C = \sum_{u=0}^{n-1} \frac{\sigma_u^z - I}{2} + \lambda \sum_{(u,v) \in E} \frac{I - \sigma_u^z - \sigma_v^z + \sigma_u^z \sigma_v^z}{4}$	$H_C = \sum_{u=0}^{n-1} \frac{\sigma_u^z - I}{2}$
$ s\rangle$ is the ground state of H_B ?	Yes	No requirement
Hilbert space	Including feasible and infeasible states	Feasible states

$d(v)$) [50, 51]. To minimize the required qubits and reduce the overhead of implementing multi-qubit controlled RX gates, an ideal subgraph should not only have the same MIS solution as the target graph but also be small and sparse (i.e., with fewer edges and where the number of edges is less than the square of the number of nodes). Constructing an ideal subgraph is a key aspect of PQA. The following sections introduce the rules for constructing induced subgraphs and methods for estimating whether they share the same MIS solution as the target graph.

A. The construction rules of the subgraph

To construct such an ideal subgraph, PQA starts from a sparse and small-sized initial subgraph G_0 and gradually expands it. During each expansion, the process favors adding the node with the lowest “closeness” to minimize the effect of the new node on the sparsity of the subgraph. The closeness is measured by a classical objective function

$$C(v_c) = \sum_{v_c \in V_c, v_q \in V_q} E(v_c, v_q), \quad (12)$$

where $V_c = V - V_q$ is the vertex candidate set, and V_q is the vertex set of the current induced subgraph G_q . If the nodes v_c and v_q are adjacent (i.e., $(v_c, v_q) \in E$), $E(v_c, v_q) = 1$. Otherwise, $E(v_c, v_q) = 0$. The value of $C(v_c)$ measures how the addition of vertex v_c to the current subgraph G_q affects its sparsity, and a small value of $C(v_c)$ indicates a minimal change in sparsity.

The choice of G_0 is not random, and it also involves the selection of the initial node in addition to graph expansion (i.e., the addition of new vertices and edges). The detailed selection rules are as follows.

The choice of the first node. To construct a sparse initial subgraph G_0 , the node with a minimum degree in the target graph G is chosen as the first node of G_0 . If there are $l (> 1)$ nodes with a minimum degree, one is randomly chosen as the first node.

The extension of subgraph. The addition of new nodes should have minimal impact on graph sparsity. That is, the node that has $\min C(v_c)$ in the candidate set is the next vertex to join the current subgraph. If there are $l (> 1)$ nodes with $\min C(v_c)$, further calculations are performed. Specifically, for each node with $\min C(v_c)$, we assume it is added to the current subgraph and calculate its corresponding $\min C(v_c)$, resulting in l calculation re-

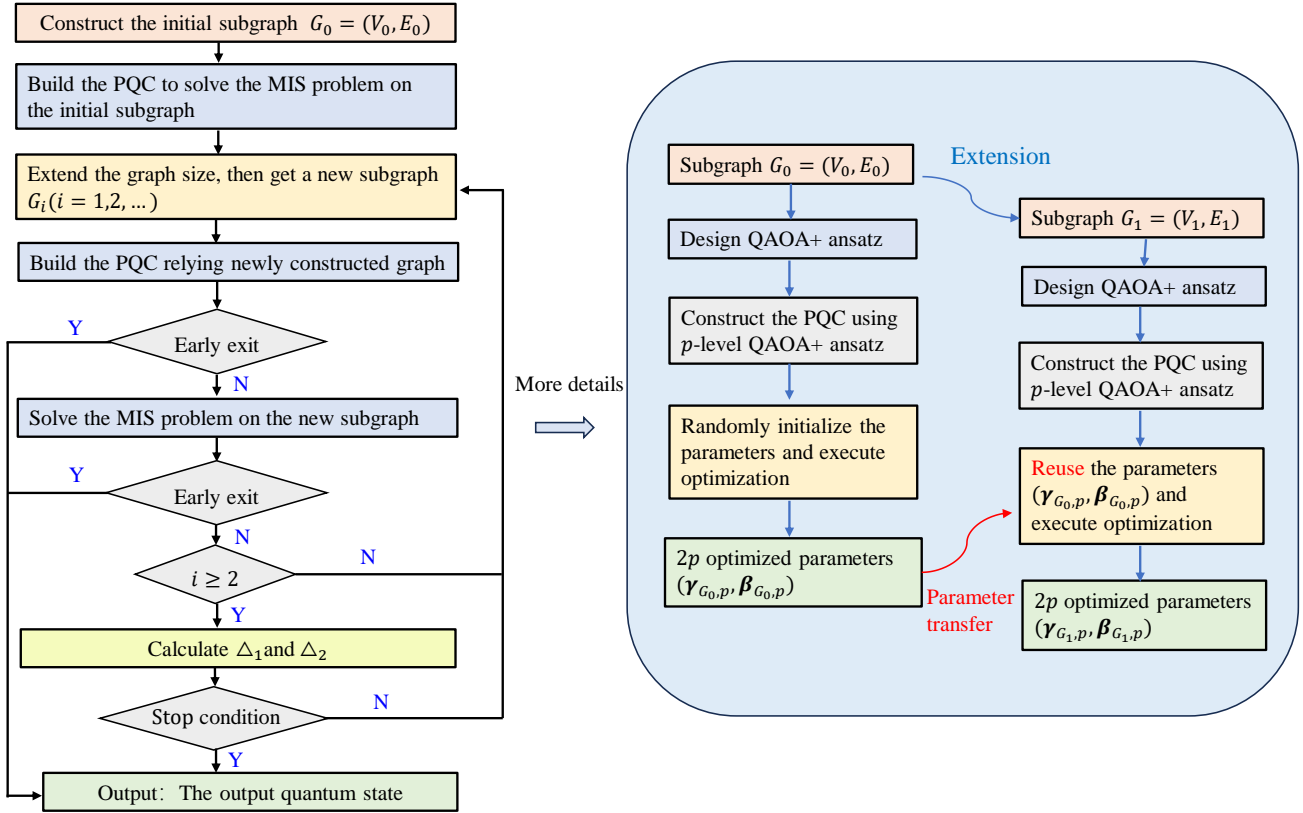


FIG. 4. A procedure schematic for PQA. PQA starts with an initial subgraph G_0 and solves the MIS problem using p -level QAOA+ ansatz, where the parameters of PQC are randomly initialized. Then, PQA progressively enlarges the graph and solves the MIS problem on the updated subgraph, retraining the PQC with pre-trained parameters. Notably, PQA incorporates two early exit mechanisms to terminate ineffective optimization, conserving quantum resources. The first mechanism assesses whether the current optimization process should proceed. The second mechanism evaluates whether further graph expansion is necessary. If the first mechanism is triggered, the PQC outputs the quantum state obtained from the previous subgraph G_{i-1} . The output state that corresponds to the maximal $F_{G_j,p}$ ($j = 0, 1, \dots, i$) is given when the second mechanism is triggered. Otherwise, the quantum state is obtained from the current subgraph G_i when the stop condition is met.

sults. The node with the minimum value among these results is chosen to expand the current subgraph. If multiple nodes meet this criteria, one is randomly selected as the next node. During the extension, new edges may be introduced. Specifically, any edge (v_q, v_{new}) should be added to the current subgraph if the newly added node v_{new} is adjacent to existing nodes v_q , resulting in an expanded subgraph.

Additionally, an example is provided in **Appendix A** to help readers understand the process of graph expansion.

B. Progressive quantum optimization

After constructing an initial induced subgraph G_0 , PQA builds a parameterized quantum circuit using the p -level QAOA+ ansatz to solve the MIS problem on G_0 , with the parameters randomly initialized. After optimization, PQA continues to expand the graph size according to the given expansion rules and constructs p -level QAOA+ ansatz for the new subgraph to solve the

MIS problem. At this stage, the PQC reuses the optimized QAOA parameters from the previous subgraph and re-optimizes these pre-trained parameters. This process is referred to as “parameter transfer” [29, 45, 52–55]. After each optimization round, PQA gets an expectation function value $F_{G_i,p}$ about the subgraph G_i , and PQA terminates if the values satisfy $\Delta_1 \leq \xi$ and $\Delta_2 \leq \xi$ or if the size matches that of the target graph in the worst case, where

$$\begin{aligned} \Delta_1 &= |F_{G_{i+1},p} - F_{G_i,p}|, \\ \Delta_2 &= |F_{G_i,p} - F_{G_{i-1},p}|. \end{aligned} \quad (13)$$

Here, ξ is the tolerance for function values, and $F_{G_i,p}$ ($F_{G_{i-1},p}$) represents the function value obtained using p -level QAOA+ ansatz to solve the MIS problem on the current (previous) subgraph G_i (G_{i-1}).

Here, we explain why $\Delta_1 \leq \xi$ and $\Delta_2 \leq \xi$ are used as the termination conditions. According to the properties of the MIS problem, adding a new vertex to the derived subgraph G_i can cause the newly constructed subgraph

G_{i+1} to have an identical or larger independence number compared with G_i . In other words, $\beta(G_i) \leq \beta(G_{i+1})$ (i.e., $F_{\max, G_i} \leq F_{\max, G_{i+1}}$). When PQA starts with a subgraph that has the same MIS solution as the target graph, the growth in the maximal expected function values F_{\max, G_i} will cease as the subgraph grows (i.e., F_{\max, G_i} reaches a steady value). Nevertheless, the value of F_{\max, G_i} might also ascend with the increase of the graph size after a brief period of stagnation when PQA starts with a different initial subgraph. During the transient stationary phase, the addition of new nodes provides no benefit (i.e., without incrementing the maximal expectation function value). This occurs due to being trapped in a local subgraph, which is affected by sub-optimal node selection. For the latter case, the subsequent enlargement of the graph might enhance performance, but it concurrently requires more quantum resources to construct the corresponding quantum circuits. At this time, scaling the graph size without regard to resources is not advisable, and PQA should terminate the process in a timely manner. Given these considerations, we prioritize the stable phase of change in the expected function value during optimization, and PQA is halted if the expected function value remains stable over three consecutive optimization rounds. By this stage, we may have discovered a derived subgraph that includes the MIS solution of the target graph, obtaining an approximate or exact solution by solving the MIS problem on this subgraph.

The quality of reused parameters can affect the optimization result for each subgraph. During actual optimization, the expectation function value may oscillate back and forth with increasing subgraph size when the parameter transfer performs poorly, delaying the fulfillment of the stop condition, such as shown in **Appendix B**. In such cases, PQA may not satisfy the termination condition and continue to execute optimization until reaching the same scale as the target graph, even though a subgraph with the same solution as the target graph has been constructed. This contradicts the original goal of PQA. To reduce running costs in PQA, we first aim to improve the quality of reused parameters by a greedy approach, as done in Ref. [56, 57], when solving the MIS problem of G_0 . Specifically, we can execute c rounds of optimization when PQA solves the MIS problem on the initial induced subgraph, then select one set of the optimized parameters with the maximal function value in c sets of results. The preserved parameters are reused to solve the MIS problem in the next subgraph. In addition, early exit mechanisms are required to end the low-cost optimization when appropriate. These mechanisms are based on evaluating the quality of the reused parameters and the optimization results for each subgraph. After each graph extension, we first decide whether to proceed with the optimization round by assessing the quality of the reused (initial) parameters. Generally, PQA can converge to quasi-optima after a few iterations (or even no optimization) when it

starts with high-quality initial parameters. Otherwise, it may require abundant iterations to converge or get stuck in a low-quality local solution. Thus, we terminate PQA early and skip the current optimization round if the expected function value, based on the initial parameters, is significantly lower than that obtained from the previous subgraph's optimization. If the quality of the initial parameters meets the rules we set, a new round of early exit judgments is carried out after the optimization. If the latest expected function value is significantly lower than the maximal value obtained from previous subgraphs, it indicates that the optimization has fallen into a poor local solution. At this time, PQA will halt further graph expansion and optimization, returning the maximal function value in this run and the corresponding output state. Otherwise, PQA continues to execute if it satisfies the above settings. In summary, to reduce the resources required during a PQA run, we introduced two early exit mechanisms that determine whether subsequent optimization rounds are necessary based on ‘flags’ (the quality of the initial parameters and the optimization results). Notably, PQA cannot get the optimal solution to the problem through an optimization run, and it simply aims to obtain a quasi-optimal solution with as few quantum resources as possible. More detailed procedures of PQA are shown in FIG. 4.

PQA is a hybrid quantum-classical algorithm, where this concept encompasses two aspects. Firstly, when the QAOA+ algorithm is used to solve the MIS problem on a subgraph, the classical computer handles parameter optimization, while the quantum computer computes the expected function value. This constitutes an external parameter optimization loop, achieving synergy between classical and quantum computation. Secondly, in constructing the subgraph, the classical computer creates a new subgraph based on the structural information of the target graph. Meanwhile, the quantum computer solves the MIS problem on the subgraph and informs the classical computer whether to continue expanding the subgraph based on the optimization results. This forms another collaborative process. In summary, PQA leverages the parallel computing capabilities of the quantum computer to solve the MIS problem on each subgraph, while sharing part of the costs (such as obtaining target graph information and parameter adjustment) with the classical computer, rather than having either the quantum or classical computer handle all resource overheads alone.

IV. RESULTS

In our work, the effects of graph construction rules and the initial graph size n_0 on the performance of PQA are first investigated in Section IV A. Then, we compare the performance of different strategies on various graphs, with more details in Section IV B.

A. The effects of graph construction rules and n_0 on the performance of PQA

To investigate the impact of graph construction rules and the initial graph size n_0 on the performance of PQA, we randomly generate multiple ER graphs. For the given graph instances, we conduct $100 \times p$ runs of PQA following various graph construction rules, where $n_0 = 1$, $\xi = 0.1$, and the quantum state $|s\rangle$ is initialized as $|\mathbf{0}\rangle$ at each solving process. Subsequently, we calculate the achieved AR by PQA at level $p = 1$ under different construction rules. Notably, the AR is the ratio between the expectation function value obtained by PQA on the final induced subgraph and $F_{\max,G}$. Here, $F_{\max,G}$ denotes the maximal expectation function value on the target graph, equivalent to the independence number of the target graph. The AR is less than or equal to one, and an AR of one signifies that PQA achieves the MIS solution of the target graph by solving the MIS problem on the current subgraph.

1. The effects of construction rules on the performance of PQA.

For each graph instance, we first calculate the optimal and average approximation ratio (OAR, AAR) obtained by multiple optimization runs of PQA when it constructs subgraphs according to different rules. Then, we average the obtained OAR and AAR across all graph instances to get the overall average OAR and AAR for PQA. From these simulation results given in FIG. 5, we observe that the expansion rules play a more significant role in the performance of PQA compared with the choice of the first node. Specifically, PQA achieves a much higher AR when following our expansion rules instead of random expansion. Given these phenomena, we analyze the variation of the expected function value during optimization and find that the parameter transfer tends to perform poorly (i.e., getting stuck in a low-quality local solution) when random vertex additions cause significant changes in the graph structure, leading to early termination of the optimization run. This may occur because significant changes in the graph structure lead to drastic shifts in the function landscape, rendering the transferred parameters suboptimal for the new landscape. In addition, FIG. 6 provides the total number of iterations required by PQA under various construction rules while achieving their respective OAR at $p = 1$. These findings suggest that PQA requires far fewer iterations to obtain a quasi-optimal solution when following our graph expansion rules, with a 95% reduction in iterations compared with random first node and expansion (i.e., 'NN'). In summary, the results presented in FIG. 5 and FIG. 6 collectively demonstrate the efficiency of our proposed graph construction rules.

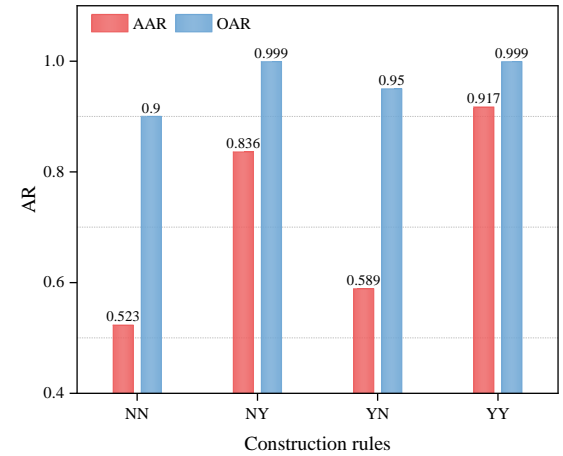


FIG. 5. The effects of graph construction rules on the AR achieved by PQA, where 'NN' suggests PQA arbitrarily chooses the first node and subsequent nodes without any rules. 'NY' represents that the first node is randomly chosen, while other newly added nodes obey our predetermined expansion rules.

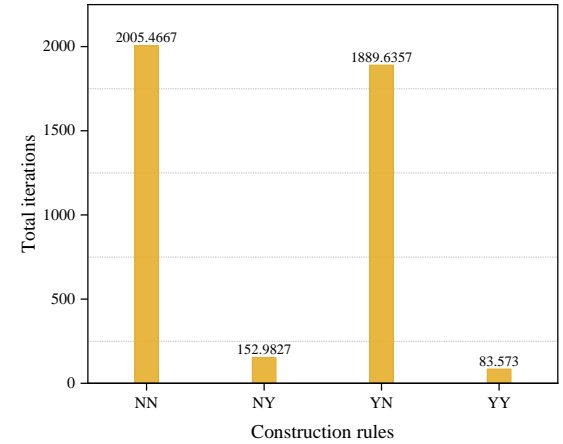


FIG. 6. The effects of graph construction rules on the total consumption of iterations to get the quasi-optimal solution.

2. The effects of n_0 on the performance of PQA.

Furthermore, we explore the impact of n_0 on the performance of PQA under various p . In our simulations, we vary the level depth from one to five and perform $100 \times p$ runs of PQA at each level. The resulting AR versus the level depth and n_0 is depicted in FIG. 7. These simulation results suggest that PQA may require more level depths to get the exact solution when the initial problem size is large. Concretely, PQA can achieve the exact MIS solution (i.e., OAR = 1) at $p = 1$ when starting with initial subgraphs of size $n_0 = 2, 4, 6$, while for PQA with $n_0 = 14$ (i.e., DS-QAOA+), its required level depth is at least five.

In general, the algorithm often requires multiple optimization runs at specific level depths to obtain the exact solution or reach a given OAR threshold. During

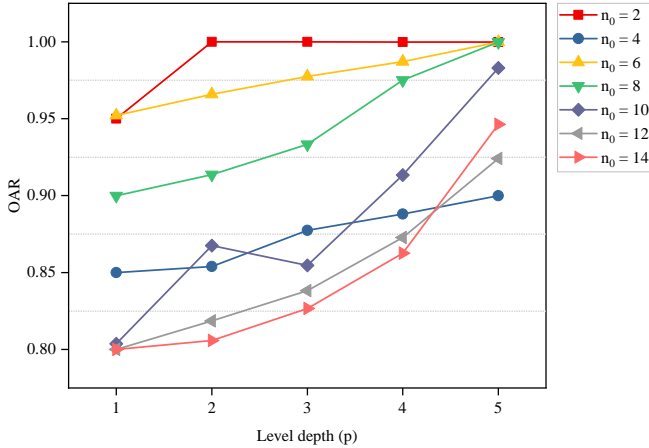


FIG. 7. The OAR achieved by PQA at various level depths p and n_0 on given ER graphs, where n_0 is the number of nodes in the initial induced subgraph G_0 . Each solid dot in the curve represents the AR obtained by PQA at level depth p when it starts from a subgraph with n_0 . Specifically, the curve reflects the AR obtained by DS-QAOA+ under various level depths when $n_0 = 14$.

parameter optimization, each run consists of numerous iterations, with each iteration requiring multiple calls to the quantum processing units (QPUs) to compute the expectation function value. More iterations increase the demand on QPUs. To comprehensively examine the effect of n_0 on the performance of PQA, we analyze the total number of optimization runs (TRs) and iterations (TITRs) when PQA initializes from various n_0 values and achieves a given OAR at the required level depths (RLDs). Specifically, for each graph instance, we first calculate the OAR achieved by multiple runs at each level depth to determine the required level depths for each algorithm to reach the given OAR. Then, we calculate the number of runs Q when the resulting AR exceeds the given OAR threshold over multiple optimization runs. We regard the ratio of Q to the total number of runs R at level depth p as the probability of exceeding that threshold. The reciprocal of this probability gives the TRs required for the algorithm to reach the given OAR. In addition, we calculate the average iterations (AITRs) needed for an optimization run at the RLDs, and the TITRs required for the algorithm to achieve the given OAR at the RLDs equals the product of TRs and AITRs. For each graph instance, we conduct a similar analysis to obtain the RLDs, TRs, and TITRs. For each graph type, we compute the average of multiple RLDs, TRs, and TITRs to estimate the number of level depths, total optimization runs, and total iterations required for the algorithm to achieve a given OAR when solving the MIS problem on a given graph type.

Moreover, for each graph instance, the total number of qubits (T-qubits), total circuit depths (TCDs), total multi-qubit controlled RX (T-MQCR) gates, and total quantum (T-Q) gates demanded by each algorithm are also calculated when they achieve the given OAR. Com-

bining with these indicators, we aim to clearly reflect the resource expenses for PQA with different n_0 . The circuit depth measures how many “layers” of quantum gates are executed in parallel, and all quantum gates that can be applied simultaneously in the circuit are regarded as one layer. The circuit depth reflects the execution time of the quantum calculation process [27, 58]. Deeper circuits require more time for execution, increasing the risk of noise and errors [14]. In this work, the circuit depth is obtained by directly using the DAGCircuit interface in MindSpore Quantum [59]. The gate resource refers to the number and types of quantum gates required in a quantum circuit, such as single-qubit rotation gates and multi-qubit controlled rotation (CR) gates, with the latter being more complex to implement on quantum hardware. Gate resources reflect the operational complexity of quantum circuits, with more gates generally leading to greater complexity. In our work, we count the number of single-qubit RX gates, single-qubit RZ gates, and multi-qubit controlled RX gates. The sum of these gives the consumption of quantum gates required by the PQC with the p -level QAOA+ ansatz. In our calculations, the number of $d(v)$ -qubit controlled RX gates in one level QAOA+ ansatz is incremented by one if $d(v) \geq 1$. The total quantum resources are the product of the average consumption per run and TRs at their respective RLDs.

From these simulation results shown in Table II, we observe that PQA’s resource demands increase as it starts with a larger initial induced subgraph. Specifically, PQA with $n_0 = 2$ achieves the given OAR while consuming only about 4.718% of the quantum resources required by DS-QAOA+ (i.e., PQA with $n_0 = 14$). This represents a savings of approximately 95.9% of iterations compared with DS-QAOA+, revealing substantial efficiency gains with PQA. **In conclusion, these above investigations emphasize the sensitivity of PQA to the choice of n_0 . Its performance may potentially decline when initialized with a large-scale initial subgraph.** To maintain robust performance in subsequent simulations, we opt for $n_0 = 2$. This decision is informed by our observation that smaller values of n_0 tend to yield more reliable results, ensuring the stability and effectiveness of PQA across varied scenarios.

B. The performance comparison among different algorithms

1. The OAR obtained by different algorithms under the same number of optimization runs and level depth.

In our simulations, we randomly generate 20 graphs each for different ER graphs (with probability = 0.4, 0.5) and k -regular graphs ($k = 2, 3$) with the number of nodes $n = 14$. Subsequently, we respectively test the performance of PQA, QLS, and DS-QAOA+ on these graphs. For PQA, the tolerance on function values $\xi = 0.1$ and

TABLE II. The required level depths (RLDs), total number of optimization runs (TRs), total iterations (TITRs), total qubits (T-qubits), total circuit depths (TCDs), total multi-qubit CR (T-MQCR) gates, and total quantum (T-Q) gates for PQA to achieve the given OAR under different values of n_0 .

OAR	n_0	RLDs	TRs	TITRs	T-qubits	TCDs	T-MQCR gates	T-Q gates
0.9	2	1	1.5562	76.0375	8.7926	23.568	6.6096	17.5852
	4	3.2	8.4233	704.2204	74.54	1079.1239	340.6935	716.1204
	6	1.6	1.4397	95.0968	11.5176	66.9053	21.2897	43.2461
	8	2.4	1.9594	125.2674	20.1942	152.0068	49.0538	98.1076
	10	3.4	4.1255	294.5122	49.5827	489.149	158.6944	317.3888
	12	4.2	7.1945	549.2766	100.3954	1507.5039	490.7771	981.5542
	14	4.8	46.8667	2387.0363	656.13332	14169.9319	4613.4662	9226.9324
	2	1	1.5562	76.0375	8.7926	23.568	6.6096	17.5852
0.85	4	3	9.7833	832.7083	94.7	1252.4839	397.3335	829.4004
	6	1.4	1.5901	98.982	12.7205	67.6558	21.5299	43.7264
	8	2.2	1.9921	125.2955	20.8618	150.6104	48.6473	97.2946
	10	3.2	4.783	371.4308	60.6338	584.0127	189.7596	379.5192
	12	4.0	5.5698	426.9543	77.7713	1125.6186	366.4565	732.913
	14	4.6	33.0571	1521.2784	462.8	7244.8851	2358.7998	4717.5996

the quantum state $|s\rangle$ is initialized as $|0\rangle$ at each solving process. The classical outer parameter optimization loop ends when the convergence tolerance [27] satisfies $\varepsilon \leq 0.001$.

We set the level depth from one to five, and each algorithm is executed $100 \times p$ optimization runs at each depth. At the end of the runs, we calculate the OAR achieved by each algorithm. These experimental procedures yield 20 sets of OAR for each graph type. The mean value of these sets provides the average OAR for various algorithms at depth p . From these numerical results illustrated in FIG. 8, we observe that the achieved OAR tends to increase as the level depth increases, thereby enhancing the quality of the obtained solution. **More importantly, these numerical results demonstrate that the OAR achieved by PQA is superior to that obtained by DS-QAOA+ and QLS at the same level depth and number of optimization runs.** More specifically, on the ER graphs with prob = 0.4, the OAR achieved by PQA is approximately 8.24% (13.668%) higher than that achieved by QLS (DS-QAOA+). On the ER graphs with prob = 0.5, the OAR achieved by PQA is approximately 8.128% (14.422%) higher than that achieved by QLS (DS-QAOA+). On the 2-regular graphs, the OAR achieved by PQA is about 3.612% (4.514%) higher than that achieved by QLS (DS-QAOA+). On the 3-regular graphs, the OAR obtained by PQA is about 8.486% and 9.438% higher than that

achieved by QLS and DS-QAOA+, respectively.

2. The quantum resources consumed by various algorithms when they achieve the same OAR.

To provide a more comprehensive comparison of the performance of DS-QAOA+, QLS, and PQA, we further investigate the total number of optimization runs and iterations required by each algorithm to reach a given OAR at the required level depths. Moreover, for each graph instance, the total number of qubits, total circuit depths, and other resources demanded by each algorithm are also calculated. These indicators are used to clearly demonstrate the resource consumption of each algorithm when they reach the same OAR.

In the numerical simulation experiments, we set the level depth from one to n , and the OAR obtained by each algorithm under multiple runs to be at least 0.95. We perform 100 optimization runs at each level depth p when $p \leq 5$, and 2^p optimization runs when $p > 5$. For each graph instance, we calculate the RLDs, TRs, ITRs, and other resources when they achieve the OAR of 0.95. Averaging the data of the same graph type provides an estimate of the resources consumed by different algorithms when solving the MIS problem on various graph types to achieve the given OAR. The specific numerical results are shown in Table III. These results suggest that

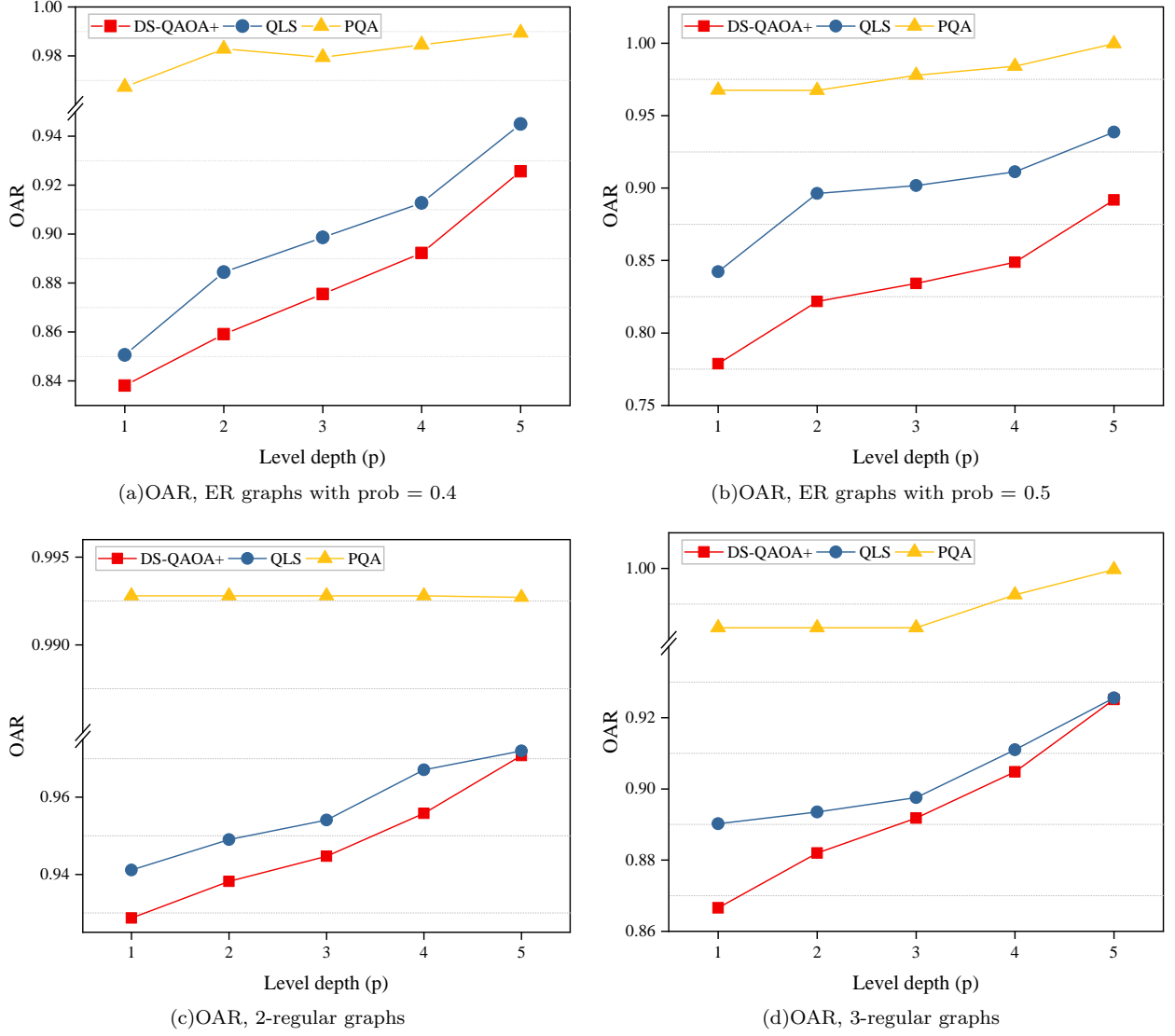


FIG. 8. The AR achieved by PQA, QLS, and DS-QAOA+ under the same level depth and optimization runs. In each subplot, the curves depict the AR achieved by the different algorithms across various graph types as the level depth p increases.

PQA is usually able to achieve the OAR of 0.95 with fewer resources. Table IV summarizes the quantum resources saved by PQA relative to DS-QAOA+ and QLS when an OAR of 0.95 is reached on a given graph type. For example, when solving the MIS problem on a 2-regular graph, the total qubits consumed by PQA is only 28.63% of DS-QAOA+, saving 71.37% in qubit usage. These results demonstrate that PQA not only achieves the given OAR of 0.95 in fewer optimization runs and iterations but also significantly reduces the consumption of qubits, circuit depth, and quantum gates compared with DS-QAOA+ and QLS, highlighting its efficiency. By minimizing the quantum resources required while maintaining high performance, PQA may be increasingly promising for practical implementation in scenarios where resource availability is limited. In our work, we also test other OAR thresholds (i.e., 0.8, 0.85, and 0.9) and show the

corresponding resources required by each algorithm in the Appendix C.

3. The comparison of the running time when DS-QAOA+, QLS, and PQA achieve the same OAR.

To assess the performance of different algorithms in achieving the given OAR, we examine the resource consumption of QLS, PQA, and DS-QAOA+. Experimental results show that QLS and PQA typically require fewer resources than DS-QAOA+ to achieve the same OAR. For QLS and PQA, classical computations (i.e., determining whether an edge exists between two points) are involved in updating the global solution and graph expansion. In contrast, DS-QAOA+ excludes such computations. Although numerical simulations show that the

TABLE III. The required level depths (RLDs), the total number of optimization runs (TRs) and iterations (TITRs), total qubits (T-qubits), total circuit depths (TCDs), total multi-qubit CR (T-MQCR) gates, and total quantum (T-Q) gates consumed by different algorithms on specific graph types when they achieve OAR of 0.95.

Types	Algo.	RLDs	TRs	TITRs	T-qubits	TCDs	T-MQCR gates	T-Q gates
ER, prob = 0.4	DS-QAOA+	4.9	91.6192	5664.43	1282.669	19304.17	6285.077	12570.15
	QLS	4.4	26.8412	1666	371.46	5282.35	1648.8952	3297.79
	PQA	1.35	17.7572	1652	112.76	464.35	135.84	337.3868
ER, prob = 0.5	DS-QAOA+	6.85	339.1095	21624	4747.533	99884.7	32520.6	65041.2
	QLS	4.55	34.3853	1939.38	478.59	7011.16	2186.785	4373.57
	PQA	1.6	15.8492	1241.81	110.94	527.78	160.869	361.362
2-regular	DS-QAOA+	3.35	10.4152	735.41	145.813	1500.31	488.473	976.946
	QLS	2.35	5.35	374.34	50.02	655.375	202.498	405
	PQA	1	5.15	336.96	41.74	91.89	22.497	83.48
3-regular	DS-QAOA+	6.3	493.9459	36313	6915.243	133809.9	43566.03	87132.06
	QLS	6.21	50.3033	3519.34	690.37	14005.5	4359.867	8719.735
	PQA	1.35	20.5773	2319.783	150.21	482.54	125.522	407.431

TABLE IV. The ratio of quantum resources saved by PQA relative to DS-QAOA+ and QLS when an OAR of 0.95 is achieved.

Types	Algo.	RLDs	TRs	TITRs	T-qubits	TCDs	T-MQCR gates	T-Q gates
ER, prob = 0.4	DS-QAOA+	0.7245	0.8062	0.7083	0.9121	0.9759	0.9784	0.9732
	QLS	0.6932	0.3384	0.0084	0.6964	0.9121	0.9176	0.8977
ER, prob = 0.5	DS-QAOA+	0.7664	0.9533	0.943	0.9766	0.9947	0.9951	0.9944
	QLS	0.6484	0.5391	0.36	0.7682	0.9247	0.9264	0.9174
2-regular	DS-QAOA+	0.7015	0.5054	0.5418	0.7137	0.9388	0.9539	0.9145
	QLS	0.5745	0.0379	0.1	0.1655	0.8598	0.8889	0.7939
3-regular	DS-QAOA+	0.7857	0.9583	0.9361	0.9783	0.9964	0.9971	0.9953
	QLS	0.7826	0.5909	0.3408	0.7824	0.9655	0.9712	0.9533

time for a single edge judgment is minimal, we include this classical computation time in our runtime comparison for fairness.

For QLS and PQA, the time required for a single optimization run includes both quantum and classical components. The classical time T_c is the time consumed in determining whether there is an edge between vertices during updating the global solution or expanding the sub-graph. Assuming that the time required for a single determination is t_j , and the total number of determinations required by the algorithm in one run is TJ , then

$$T_c = TJ \times t_j. \quad (14)$$

The quantum running time T_q includes the time re-

quired for initial state preparation, quantum state measurements, and quantum gate evolution across multiple iterations [58]. In each iteration, M repeated measurements are needed to calculate the average expectation value of the objective function. The time consumed in a single repetition is

$$t_q = t_p + t_M + (\text{circuit depth}) \times t_G, \quad (15)$$

where t_p is the initial state preparation time, t_M is the time for a single measurement, t_G is the time for a single quantum gate evolution, and circuit depth is the depth of the parameterized quantum circuit. The time consumed for a single iteration is

$$T_{ITR} = t_q \times M, \quad (16)$$

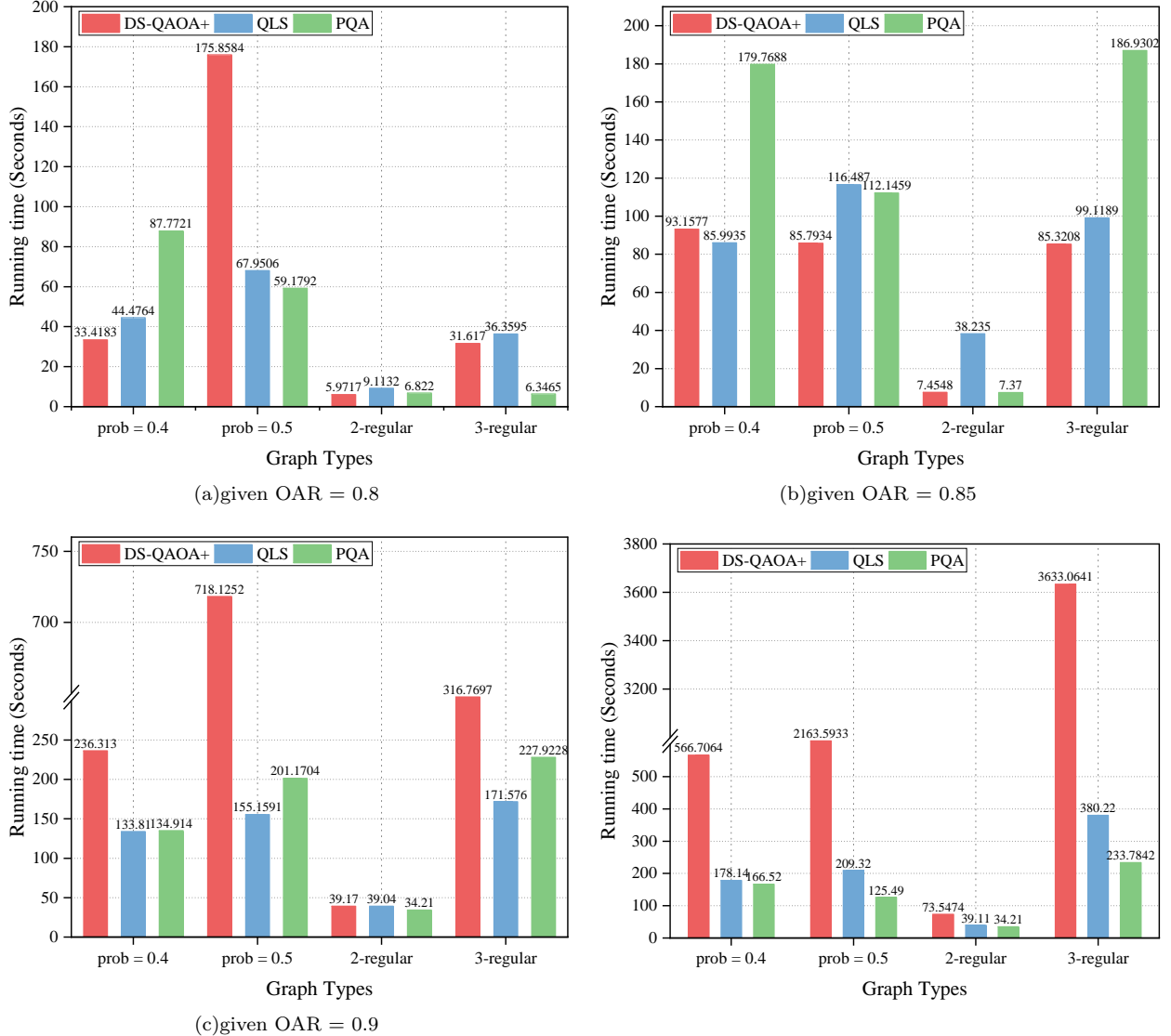


FIG. 9. The required running time of DS-QAOA+, QLS, and PQA when they achieve the same given OAR.

and the quantum time consumed in a single optimization run is

$$T_q = T_{ITR} \times \text{ITRs}, \quad (17)$$

where ITRs is the number of iterations required for the objective function to converge in this run. Therefore, the time consumed in a single run for QLS and PQA is

$$T_{PQA} = T_{q,PQA} + T_{c,PQA}, \quad (18)$$

$$T_{QLS} = T_{q,QLS} + T_{c,QLS}, \quad (19)$$

respectively, while for DS-QAOA+, its running time is

$$T_{DS} = T_{q,DS}. \quad (20)$$

This study explores the runtime required by differ-

ent algorithms to achieve the same OAR across various graph types. The calculations employ the same realistic assumptions as Ref. [58], namely, $t_p + t_M$ is one millisecond, and t_G is 10 nanoseconds. The tests are conducted on a server equipped with an Intel(R) Xeon(R) Sliver 4316 CPU running at 2.3GHz and 251GB of RAM, where t_j is determined to be 0.31226 milliseconds. Numerical simulations in FIG. 9 show that when the given OAR is 0.8 (0.85, 0.9), the runtime of PQA on certain graph types may be slightly higher than that of QLS and DS-QAOA+. However, as shown in Table A1 in Appendix C, PQA requires only a fraction of the qubits to achieve the given OAR compared with QLS and DS-QAOA+. Moreover, as the given OAR increases (i.e., as the quasi-optimal solutions approach the true solution), PQA consumes less runtime than DS-QAOA+ and QLS, while also requiring fewer qubits, multi-qubit controlled rotation gates, and other resources. Numerical results

suggest that PQA exhibits various advantages at different OARs and graph types, such as reduced qubit consumption, shorter runtime, or both. **In summary, while PQA may not always be the optimal choice for all OARs and graph types, it likely achieves better results with less runtime and resource consumption compared to DS-QAOA+ and QLS when targeting higher-quality solutions.**

V. CONCLUSIONS

This paper proposes PQA to reduce quantum resource consumption in the application of QAOA+ for solving the MIS problem. The core idea of PQA is to progressively construct a subgraph containing the MIS solution. As a result, solving the MIS problem on this subgraph provides the MIS solution for the target graph. By doing so, PQA can achieve a quasi-optimal solution with reduced resource consumption compared with conventional approaches like DS-QAOA+. Thus, leveraging PQA on NISQ devices may enable solving larger and more complex optimization problems within current resource constraints.

Our analysis examines the impact of n_0 (the number of vertices in the initial subgraph) on both the final AR achieved by PQA and its quantum resource consumption. The results suggest that starting with a large initial subgraph may lead to a performance decline in PQA. To simplify, PQA starts with a small subgraph and adds one node during each graph extension. However, this incremental approach may introduce unnecessary optimization rounds, increasing the iteration count. To overcome this limitation and streamline the optimization process, future research should explore more effective graph construction methods and the optimal choice of initial size n_0 , taking into account the graph structure to maintain PQA performance. A potential way to reduce optimization rounds is by adding multiple vertices during each expansion, but further investigation is needed to understand its impact on PQA performance. Another promising approach is integrating machine learning to optimize the selection of n_0 and dynamically adjust the graph expansion strategy based on real-time feedback. These advancements could significantly reduce iterations in the external optimization loop, improving the overall efficiency and scalability of PQA for quantum optimization problems.

The graph structure plays a role in determining the performance of PQA. Designing more refined and efficient graph expansion rules for specific graph types is essential. This could further enhance the performance of PQA in future applications. Notably, PQA has potential applications in a broader range of constrained combinatorial optimization problems, although this paper focuses on the MIS problem as an example. When extending PQA to tackle various optimization problems, it is crucial

to investigate the optimal subgraph construction scale for specific problems. Thus, future research should focus on exploring optimal subgraph construction rules for different problem instances. These investigations may provide valuable insights for fine-tuning PQA and improving its performance and applicability across various combinatorial optimization problems.

ACKNOWLEDGEMENTS

This work is supported by National Natural Science Foundation of China (Grant Nos. 62371069, 62372048, 62272056), Beijing Natural Science Foundation (Grant No. 4222031) and BUPT Excellent Ph.D. Students Foundation(CX2023123).

A. The extension of the subgraph

In this appendix, we introduce the process of the graph extension based on two different derived subgraphs as shown in FIG. A1.

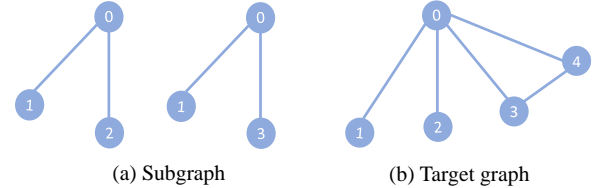


FIG. A1. The target graph and its induced subgraphs.

Denote the current subgraph as $G_i = (V_i, E_i)$. For the first subgraph in FIG. A1, $V_i = \{0, 1, 2\}$ and $E_i = \{(0, 1), (0, 2)\}$. The candidate vertex set $V_C = V - V_i = \{3, 4\}$. Our goal is to select the vertex from V_C that has the least connection with the current subgraph to be added to G_i . Specifically, if node 3 is added to G_i , $C(v_c = 3) = 1$. Similarly, if node 4 is added, $C(v_c = 4) = 1$. Since both nodes have the same connection, we proceed to the next round of selection. When node 3 is added to V_i , the edge $(0, 3)$ is included in E_i , leaving $V_C = \{4\}$ and $C(v_c = 4) = 2$. Similarly, if node 4 were added, $C(v_c = 3) = 2$. After evaluating both nodes, since they equally satisfy the selection criteria, one can be randomly added to V_i . If node 3 (or 4) is added, the edge $(0, 3)$ (or $(0, 4)$) is included in E_i . The resulting subgraph becomes is $G_{i+1} = \{\{0, 1, 2, 3\}, \{(0, 1), (0, 2), (0, 3)\}\}$ (or $G_{i+1} = \{\{0, 1, 2, 4\}, \{(0, 1), (0, 2), (0, 4)\}\}$).

For the second subgraph in FIG. A1, $V_i = \{0, 1, 3\}$ and $E_i = \{(0, 1), (0, 3)\}$. The candidate vertex set $V_C = \{2, 4\}$, with $C(v_c = 2) = 1$ and $C(v_c = 4) = 2$. We choose the node with the smallest $C(v_c)$ value from the candidate vertex set. Thus, node 2 is the next node to be added to V_i , and the edge $(0, 2)$ is added

to E_i . The newly constructed subgraph is $G_{i+1} = \{\{0, 1, 2, 3\}, \{(0, 1), (0, 2), (0, 3)\}\}$.

B. The variation of expectation function values in optimization runs of PQA

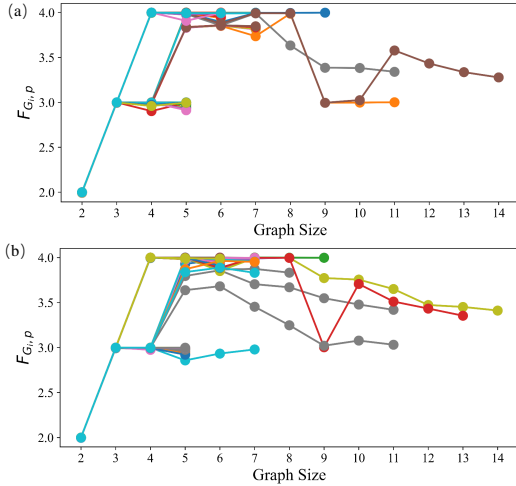


FIG. A2. The variation of expectation function values in optimization runs of PQA at level depth p , where $n_0 = 2$ and the maximal expectation function value is 4. In each subplot, each curve corresponds to an optimization run of PQA, where the square on each curve is the obtained function value after each optimization round. The X-axis represents the number of nodes in the current induced subgraph, where the maximal value of the X-axis is the maximal size of the final subgraph when PQA terminates. (a) $p = 4$, (b) $p = 5$.

In our simulations, we use PQA (without early stop mechanisms) to solve the MIS problem on an ER graph with $n = 14$ vertices, setting the level depths to $p = 4$ and $p = 5$. At each level depth, PQA performs $20 \times p$ optimization runs. This section provides detailed analysis of the changes in the expectation function value during each optimization run of PQA. From the simulation results in FIG. A2, we observe that fluctuations in the expectation function values can delay the termination of PQA. That is, more optimization rounds are required in an optimization run when the expectation function values obviously fluctuate back and forth (i.e., the values do not meet the stop condition). As a result, the final induced subgraph may reach the same size as the target graph when the optimization process of PQA concludes.

C. The quantum resources consumed by different algorithms under various given OAR.

We analyze the resource consumption of each algorithm across various graph types and at different OAR thresholds. The focus is on critical factors such as required level depths, the total number of optimization

runs, and so on. Numerical results are presented in Table A1. These data show that while PQA typically requires more iterations than QLS to achieve certain OAR thresholds on specific graph types, it consistently consumes fewer qubits, has shallower circuit depths, and uses fewer quantum gates. Table A2 further quantifies these advantages. For example, PQA saves 54.12% of qubits and 81.09% of quantum gates compared to QLS when solving the MIS problem on ER graphs (with a probability of 0.4) and reaching an OAR of 0.9. The numerical simulations reveal that resource consumption varies with the OAR threshold for each algorithm. While PQA does not consistently outperform QLS and DS-QAOA+ across all resource metrics at every threshold, our results show that between OAR thresholds of 0.8 and 0.9, PQA is the preferred choice when a moderate increase in iterations is acceptable in exchange for shallower level depths and fewer qubits. Conversely, if minimizing the number of iterations is the priority, QLS is more efficient for solving the MIS problem. Nonetheless, DS-QAOA+ usually requires more resources than both QLS and PQA.

TABLE A1. The required level depths (RLDs), the total number of optimization runs (TRs) and iterations (TITRs), and other quantum resources consumed by different algorithms on specific graph types when they achieve various given OAR.

OAR	Types	Algo.	RLDs	TRs	TITRs	T-qubits	TCDs	T-MQCR gates	T-Q gates
0.8	ER, prob = 0.4	DS-QAOA+	2.75	7.196	333.8991	100.74	850.93	277.05	554.09
		QLS	2.4	8.6584	411.3193	119.82	916.92	289.46	578.93
		PQA	1.15	12.2964	869.1626	76.24	271.75	81.16	190.59
	ER, prob = 0.5	DS-QAOA+	2.85	37.5934	1745.184	526.31	7678.45	2499.96	4999.92
		QLS	2.2	15.0766	619.6376	209.81	1466.2	462.84	925.67
		PQA	1.25	6.385	586.3698	45.65	170.48	51.4	119.4
	2-regular	DS-QAOA+	1.05	1.213	59.7134	16.98	54.77	17.83	35.66
		QLS	1.1	1.2337	88.2352	11.54	43.55	13.26	26.52
		PQA	1	1.0415	67.185	8.44	18.58	4.54	16.88
	3-regular	DS-QAOA+	1.2	7.2102	316.0523	100.94	372.05	121.13	242.26
		QLS	1.1579	8.0593	338.0899	110.61	412.3	128.42	256.85
		PQA	1	1.0683	62.5453	7.69	17.95	4.59	15.38
0.85	ER, prob = 0.4	DS-QAOA+	3.75	18.2939	928.8368	4674.59	2949.89	960.43	1920.86
		QLS	3.15	14.6076	798.6345	226.75	2037.03	641.73	1283.47
		PQA	1.2	21.0906	1782.131	104.04	523.05	158.18	362.76
	ER, prob = 0.5	DS-QAOA+	4.85	15.6669	854.652	24432.58	3839.96	1250.22	2500.44
		QLS	3.35	22.4242	1066.927	282.38	3327.75	1049.37	2098.75
		PQA	1.45	15.4684	1108.006	144.04	526.7	161.64	361.96
	2-regular	DS-QAOA+	1.15	1.361	74.5434	835.99	67.3	21.91	43.82
		QLS	1.25	6.1747	367.6252	48.16	257.79	79.34	158.69
		PQA	1	1.1305	72.5766	41.75	20.17	4.94	18.33
	3-regular	DS-QAOA+	3.65	15.6257	851.1209	4424.73	2452	798.47	1597
		QLS	3.3684	16.6128	913.7158	282.41	2469	778.84	1557.7
		PQA	1.3	18.0773	1853.443	150.21	409.45	106.66	345.28
0.9	ER, prob = 0.4	DS-QAOA+	4.2	39.1584	2228.736	4674.59	60302.18	19633.27	39266.53
		QLS	3.6	22.0714	1244.793	226.75	2628.11	823.03	1646.06
		PQA	1.35	16.3847	1337.357	104.04	428.46	125.34	311.01
	ER, prob = 0.5	DS-QAOA+	5.8	83.4828	4900.988	24432.58	465266.05	151481.97	302963.94
		QLS	3.9	28.0586	1426.722	282.38	3535.17	1105.62	2211.24
		PQA	1.5	20.2879	1994.846	144.04	621.82	184.62	444.31
	2-regular	DS-QAOA+	2.6	6.8045	389.1411	835.99	6675.96	2173.57	4347.14
		QLS	2.35	5.354	374.3412	48.16	459.21	143.97	287.94
		PQA	1	5.151	336.9634	41.75	91.9	22.5	83.5
	3-regular	DS-QAOA+	4.8	45.5427	2973.713	4424.73	65233.19	21238.71	42477.43
		QLS	4.5789	25.5096	1587.143	282.41	4251.92	1328.6	2657.2
		PQA	1.3	20.5773	2261.173	150.21	466.08	121.41	393.03

TABLE A2. The ratio of quantum resources saved by PQA relative to DS-QAOA+ and QLS when a given OAR is reached.

OAR	Types	Algo.	T-qubits	TCDs	T-MQCR gates	T-Q gates
0.8	ER, prob = 0.4	DS-QAOA+	0.2433	0.6806	0.7071	0.6560
		QLS	0.3638	0.7036	0.7196	0.6708
	ER, prob = 0.5	DS-QAOA+	0.9133	0.9778	0.9794	0.9761
		QLS	0.7824	0.8837	0.8889	0.8710
	2-regular	DS-QAOA+	0.5029	0.6607	0.7448	0.5266
		QLS	0.2682	0.5733	0.6569	0.3635
0.85	3-regular	DS-QAOA+	0.9238	0.9518	0.9621	0.9365
		QLS	0.9305	0.9565	0.9642	0.9401
	ER, prob = 0.4	DS-QAOA+	0.4647	0.8227	0.8353	0.8111
		QLS	0.3219	0.7432	0.7535	0.7174
	ER, prob = 0.5	DS-QAOA+	0.4746	0.8628	0.8707	0.8552
		QLS	0.6308	0.8417	0.8460	0.8275
0.9	2-regular	DS-QAOA+	0.5191	0.7003	0.7746	0.5818
		QLS	0.8413	0.9218	0.9378	0.8845
	3-regular	DS-QAOA+	0.3968	0.8330	0.8664	0.7838
		QLS	0.4212	0.8342	0.8631	0.7783
	ER, prob = 0.4	DS-QAOA+	0.9777	0.9929	0.9936	0.9921
		QLS	0.5412	0.8370	0.8477	0.8109
0.9	ER, prob = 0.5	DS-QAOA+	0.9941	0.9987	0.9988	0.9985
		QLS	0.4899	0.8241	0.8330	0.7991
	2-regular	DS-QAOA+	0.9501	0.9862	0.9896	0.9808
		QLS	0.1331	0.7999	0.8437	0.7100
	3-regular	DS-QAOA+	0.9661	0.9929	0.9943	0.9907
		QLS	0.4681	0.8904	0.9086	0.8521

[1] L. K. Grover, Phys. Rev. Lett. **79**, 325 (1997).

[2] P. W. Shor, SIAM Review **41**, 303 (1999), <https://doi.org/10.1137/S0036144598347011>.

[3] S. Lloyd, M. Mohseni, and P. Rebentrost, Nature Physics **10**, 631 (2014).

[4] C.-H. Yu, F. Gao, and Q.-Y. Wen, IEEE Transactions on Knowledge and Data Engineering **33**, 858 (2019).

[5] S.-J. Pan, L.-C. Wan, H.-L. Liu, Q.-L. Wang, S.-J. Qin, Q.-Y. Wen, and F. Gao, Phys. Rev. A **102**, 052402 (2020).

[6] L.-C. Wan, C.-H. Yu, S.-J. Pan, F. Gao, Q.-Y. Wen, and S.-J. Qin, Phys. Rev. A **97**, 062322 (2018).

[7] A. W. Harrow, A. Hassidim, and S. Lloyd, Physical review letters **103**, 150502 (2009).

[8] J. Preskill, Quantum **2**, 79 (2018).

[9] M. Cerezo, A. Arrasmith, R. Babbush, S. C. Benjamin, S. Endo, K. Fujii, J. R. McClean, K. Mitarai, X. Yuan, L. Cincio, and P. J. Coles, Nature Reviews Physics **3**, 625 (2021).

[10] K. Bharti, A. Cervera-Lierta, T. H. Kyaw, T. Haug, S. Alperin-Lea, A. Anand, M. Degroote, H. Heimonen,

J. S. Kottmann, T. Menke, *et al.*, *Reviews of Modern Physics* **94**, 015004 (2022).

[11] H. R. Grimsley, S. E. Economou, E. Barnes, and N. J. Mayhall, *Nature communications* **10**, 3007 (2019).

[12] H. L. Tang, V. Shkolnikov, G. S. Barron, H. R. Grimsley, N. J. Mayhall, E. Barnes, and S. E. Economou, *PRX Quantum* **2**, 020310 (2021).

[13] D. Zhu, N. M. Linke, M. Benedetti, K. A. Landsman, N. H. Nguyen, C. H. Alderete, A. Perdomo-Ortiz, N. Korda, A. Garfoot, C. Brecque, *et al.*, *Science advances* **5**, eaaw9918 (2019).

[14] Y. Du, T. Huang, S. You, M.-H. Hsieh, and D. Tao, *npj Quantum Information* **8**, 62 (2022).

[15] Z. He, M. Deng, S. Zheng, L. Li, and H. Situ, in *Proceedings of the AAAI Conference on Artificial Intelligence*, Vol. 38 (2024) pp. 12430–12438.

[16] Y. Song, Y. Wu, S. Wu, D. Li, Q. Wen, S. Qin, and F. Gao, *Science China Physics, Mechanics & Astronomy* **67**, 250311 (2024).

[17] Y. Wu, B. Wu, J. Wang, and X. Yuan, *Quantum* **7**, 981 (2023).

[18] Y. Wu, Z. Huang, J. Sun, X. Yuan, J. B. Wang, and D. Lv, *Quantum Science and Technology* (2023).

[19] X. Wang, Z. Song, and Y. Wang, *Quantum* **5**, 483 (2021).

[20] H.-L. Liu, Y.-S. Wu, L.-C. Wan, S.-J. Pan, S.-J. Qin, F. Gao, and Q.-Y. Wen, *Phys. Rev. A* **104**, 022418 (2021).

[21] E. Farhi, J. Goldstone, and S. Gutmann, “A quantum approximate optimization algorithm,” (2014), arXiv:1411.4028 [quant-ph].

[22] S. Bravyi, A. Kliesch, R. Koenig, and E. Tang, *Physical review letters* **125**, 260505 (2020).

[23] L. Zhou, S.-T. Wang, S. Choi, H. Pichler, and M. D. Lukin, *Phys. Rev. X* **10**, 021067 (2020).

[24] S. H. Sack and M. Serbyn, *Quantum* **5**, 491 (2021).

[25] M. Streif and M. Leib, *Quantum Science and Technology* **5**, 034008 (2020).

[26] L. Zhu, H. L. Tang, G. S. Barron, F. A. Calderon-Vargas, N. J. Mayhall, E. Barnes, and S. E. Economou, *Phys. Rev. Res.* **4**, 033029 (2022).

[27] X.-H. Ni, B.-B. Cai, H.-L. Liu, S.-J. Qin, F. Gao, and Q.-Y. Wen, *Advanced Quantum Technologies* **7**, 2300419 (2024).

[28] Z. Zhou, Y. Du, X. Tian, and D. Tao, *Physical Review Applied* **19**, 024027 (2023).

[29] J. Wurtz and D. Lykov, *Phys. Rev. A* **104**, 052419 (2021).

[30] P. Vikstål, M. Grönkvist, M. Svensson, M. Andersson, G. Johansson, and G. Ferrini, *Phys. Rev. Appl.* **14**, 034009 (2020).

[31] Y. Zhang, X. Mu, X. Liu, X. Wang, X. Zhang, K. Li, T. Wu, D. Zhao, and C. Dong, *Applied Soft Computing* **118**, 108554 (2022).

[32] J. Wurtz and P. Love, *Phys. Rev. A* **103**, 042612 (2021).

[33] Y. Ruan, Z. Yuan, X. Xue, and Z. Liu, *Information Sciences* **619**, 98 (2023).

[34] S. Brandhofer, D. Braun, V. Dehn, G. Hellstern, M. Hüls, Y. Ji, I. Polian, A. S. Bhatia, and T. Wellens, *Quantum Information Processing* **22**, 25 (2022).

[35] T. Tomesh, Z. H. Saleem, M. A. Perlin, P. Gokhale, M. Suchara, and M. Martonosi, in *2023 IEEE International Conference on Quantum Computing and Engineering (QCE)*, Vol. 1 (IEEE, 2023) pp. 1–12.

[36] J. R. Finžgar, A. Kerschbaumer, M. J. Schuetz, C. B. Mendl, and H. G. Katzgraber, arXiv preprint arXiv:2308.13607 (2023).

[37] R. M. Karp, *Reducibility among combinatorial problems* (Springer, 2010).

[38] S. Hadfield, Z. Wang, B. O’gorman, E. G. Rieffel, D. Venturelli, and R. Biswas, *Algorithms* **12**, 34 (2019).

[39] Z. H. Saleem, *International Journal of Quantum Information* **18**, 2050011 (2020).

[40] S.-S. Wang, H.-L. Liu, Y.-Q. Song, F. Gao, S.-J. Qin, and Q.-Y. Wen, *Physica A: Statistical Mechanics and its Applications* **626**, 129089 (2023).

[41] S. Hadfield, Z. Wang, E. G. Rieffel, B. O’Gorman, D. Venturelli, and R. Biswas, in *Proceedings of the Second International Workshop on Post Moores Era Supercomputing* (2017) pp. 15–21.

[42] Z. Wang, N. C. Rubin, J. M. Dominy, and E. G. Rieffel, *Physical Review A* **101**, 012320 (2020).

[43] Z. He, R. Shaydulin, S. Chakrabarti, D. Herman, C. Li, Y. Sun, and M. Pistoia, *npj Quantum Information* **9**, 121 (2023).

[44] T. Tomesh, Z. H. Saleem, and M. Suchara, *Quantum* **6**, 781 (2022).

[45] L. Li, J. Li, Y. Song, S. Qin, Q. Wen, and F. Gao, arXiv preprint arXiv:2311.02302 (2023).

[46] L. T. Brady and S. Hadfield, arXiv preprint arXiv:2309.13110 (2023).

[47] A. Lucas, *Frontiers in physics* **2**, 5 (2014).

[48] T. Albash and D. A. Lidar, *Rev. Mod. Phys.* **90**, 015002 (2018).

[49] M. Halldórrsson and J. Radhakrishnan, in *Proceedings of the twenty-sixth annual ACM symposium on Theory of computing* (1994) pp. 439–448.

[50] R. Vale, T. M. D. Azevedo, I. Araújo, I. F. Araujo, and A. J. da Silva, arXiv preprint arXiv:2302.06377 (2023).

[51] T. Tomesh, N. Allen, and Z. Saleem, arXiv preprint arXiv:2210.04378 (2022).

[52] A. Galda, X. Liu, D. Lykov, Y. Alexeev, and I. Safro, in *2021 IEEE International Conference on Quantum Computing and Engineering (QCE)* (IEEE, 2021) pp. 171–180.

[53] R. Shaydulin, P. C. Lotshaw, J. Larson, J. Ostrowski, and T. S. Humble, *ACM Transactions on Quantum Computing* **4**, 1 (2023).

[54] J. A. Montanez-Barrera, D. Willsch, and K. Michielsen, “Transfer learning of optimal qaoa parameters in combinatorial optimization,” (2024), arXiv:2402.05549 [quant-ph].

[55] F. G. S. L. Brandao, M. Broughton, E. Farhi, S. Gutmann, and H. Neven, “For fixed control parameters the quantum approximate optimization algorithm’s objective function value concentrates for typical instances,” (2018), arXiv:1812.04170 [quant-ph].

[56] R. Shaydulin, I. Safro, and J. Larson, in *2019 IEEE High Performance Extreme Computing Conference (HPEC)* (2019) pp. 1–8.

[57] S. H. Sack, R. A. Medina, R. Kueng, and M. Serbyn, *Physical Review A* **107**, 062404 (2023).

[58] G. G. Guerreschi and A. Y. Matsuura, *Scientific reports* **9**, 6903 (2019).

[59] M. Developer, “Mindspore quantum 0.6.0,” <https://gitee.com/mindspore/mindquantum> (2021).